Cosmic Shielding Studies at MicroBooNE

THE MICROBOONE COLLABORATION

MicroBooNE, a 89 ton active volume liquid argon time projection chamber (LArTPC) located on the Fermilab's Booster Neutrino Beamline, is designed to both probe neutrino physics phenomena, and further the development of LArTPC detector technology and event reconstruction. Since MicroBooNE is located only a few meters below the ground level, without significant shielding, a large flux of cosmic rays are expected to enter the detector volume. We present detailed simulation studies performed in order to quantify cosmogenic event rates in MicroBooNE. One of the most effective ways to reduce the cosmic air shower background is to use a high-density shielding material a few meters above the detector to block or attenuate the incoming cosmic particles. The effect of such an overburden on MicroBooNE backgrounds and event rates is explored and quantified using detailed simulation studies. In particular, the effect of a 3 m concrete overburden on these backgrounds is studied in detail. Special focus is given to cosmogenic electromagnetic showers that can fake an electron-like or photon-like event and pose a serious challenge to studies involving single e/γ searches which form a primary physics goal of MicroBooNE. We find that the addition of a 3 m concrete overburden can help significantly reduce difficult-to-control backgrounds which arise from non-muon cosmic ray primaries.

Contents

1 Introduction

MicroBooNE [1] is an 89-ton active volume LArTPC (Liquid Argon Time Projection Chamber) neutrino experiment built on the Fermilab Booster Neutrino Beamline (BNB). The two main physics goals of MicroBooNE are the investigation of the low-energy excess of electron neutrino-like events seen previously by MiniBooNE [2, 3] and precision measurements of ν-Ar interactions in the 1 GeV range. A layout of the MicroBooNE detector is shown in Fig. 1. The MicroBooNE TPC is 10.4 m long, 2.3 m high, and 2.5 m wide. It consists of cathode and anode planes enclosed in a volume of highly purified liquid argon (LAr). Neutrino interactions with liquid argon in the TPC produce charged particles that cause ionization and excitation of argon. A large electric field drifts ionization charge toward finely segmented anode wire planes. In MicroBooNE, the distance between the cathode and anode is 2.56 m and an ionization electron takes about 1.6 ms to travel the full drift distance at an electric field of 500 V/cm. The total readout time for a given event in MicroBooNE is three times (four times) this 1.6 ms drift window for TPC (PMT) at 500 V/cm. This long readout time per event is required to accommodate cosmic ray tracks which are not coincident with the neutrino interaction time but are coincident with the drift window containing the neutrino interaction [4].

Since MicroBooNE is situated just below ground level (only $\sim$6 meters underground with no earth overburden), it is exposed to a large flux of cosmic rays. Estimating the portion of this cosmic flux that enters the detector and exploring ways to reduce it are crucial to successfully performing any neutrino beam-related analysis in MicroBooNE. Understanding these backgrounds is not only important for MicroBooNE but the entire surface-based Short-Baseline Neutrino (SBN) Program at Fermilab [5]. One way to reduce the cosmic air
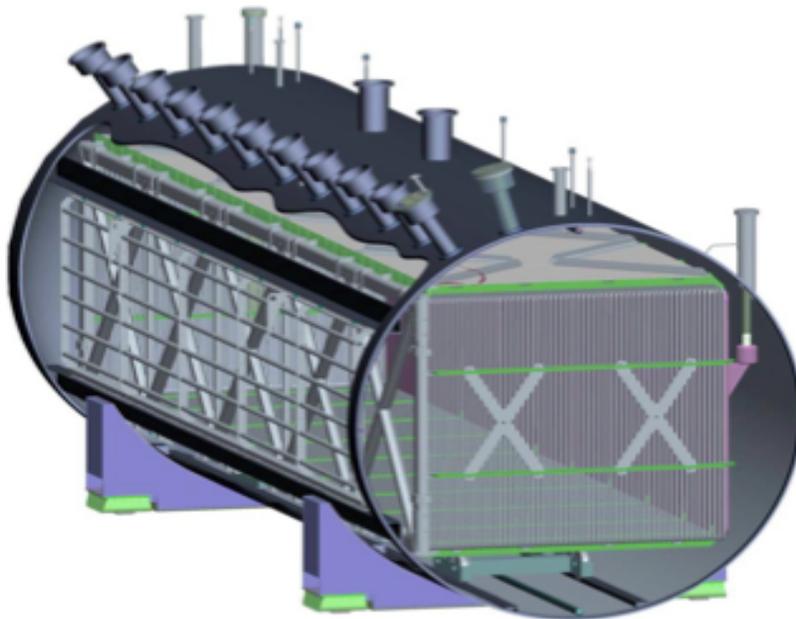

Figure 1: Layout of the MicroBooNE experiment.

shower background in surface detectors is to introduce an earth-equivalent (density-wise) overburden above the detector and in the case of MicroBooNE on the roof of the detector enclosure. The analysis and results presented in this note address the question of whether MicroBooNE requires such an overburden. Addressing this question requires understanding the size of various cosmic backgrounds that will enter the active volume of the detector. In particular, estimating the cosmic electromagnetic (EM) background is crucially important for single e/γ searches and in particular investigations of the low energy excess observed by the MiniBooNE experiment.

All the studies shown in this note are performed using detailed Monte Carlo (MC) simulations. Details about the MicroBooNE geometry and simulations including CRY [6] and CORSIKA [7] generator comparisons are given in Section 2. Estimates of particle rates expected in the detector active volume and detailed estimates of cosmic-induced electromagnetic showers are discussed in Section 3. The effect of using a 3 m concrete overburden on various backgrounds is discussed in Section 4. Section 5 gives a summary of the studies presented in the note and reiterates important observations to determine whether MicroBooNE would benefit from an overburden.

2 MicroBooNE geometry and simulation

2.1 Geometry simulation

This section briefly describes the MicroBooNE geometry that was used in the simulation studies performed for this work. MicroBooNE is located $\sim$6 m underground at Fermilab, which is at an elevation of 740.6 feet ($\sim$226 m) above mean sea level. The geomagnetic location of Fermilab corresponds to a latitude of $17°$ $22'$ $43''$ North and longitude of $78°$ $28'$ $31''$ East. The MicroBooNE geometry simulation is at a mature stage and includes detailed simulations of the detector, cryostat and surroundings. Elements that surround the detector and have non-negligible density are important for cosmic background studies since they can absorb some particles and generate additional backgrounds. For example, the electronics racks that are located just above the detector on the platform can block significant amounts of cosmic electromagnetic background, while the dense concrete experimental pit that surrounds the cryostat is capable of producing new backgrounds due to particle interactions in the concrete.

The LArTF building is designed to hold up to 3 m of concrete-equivalent overburden. The overburden simulation studied in this note assumes a uniform 3 m thick concrete disc placed above the roof of the LArTF building. Note that this assumption is valid as an approximation since multiple concrete blocks (possibly staggered to avoid clear line-of-sight paths) could be used to cover the roof of the LArTF building, so, the coverage won't be as uniform as the concrete disc. Figure 2 shows a transparent view of the MicroBooNE geometry with overburden included along with a zoomed-in view of the detector surroundings as simulated in the current geometry. For comparison, Figure 3 shows a 3D drawing of the interior of the LArTF building along with an actual photograph of what currently exists on
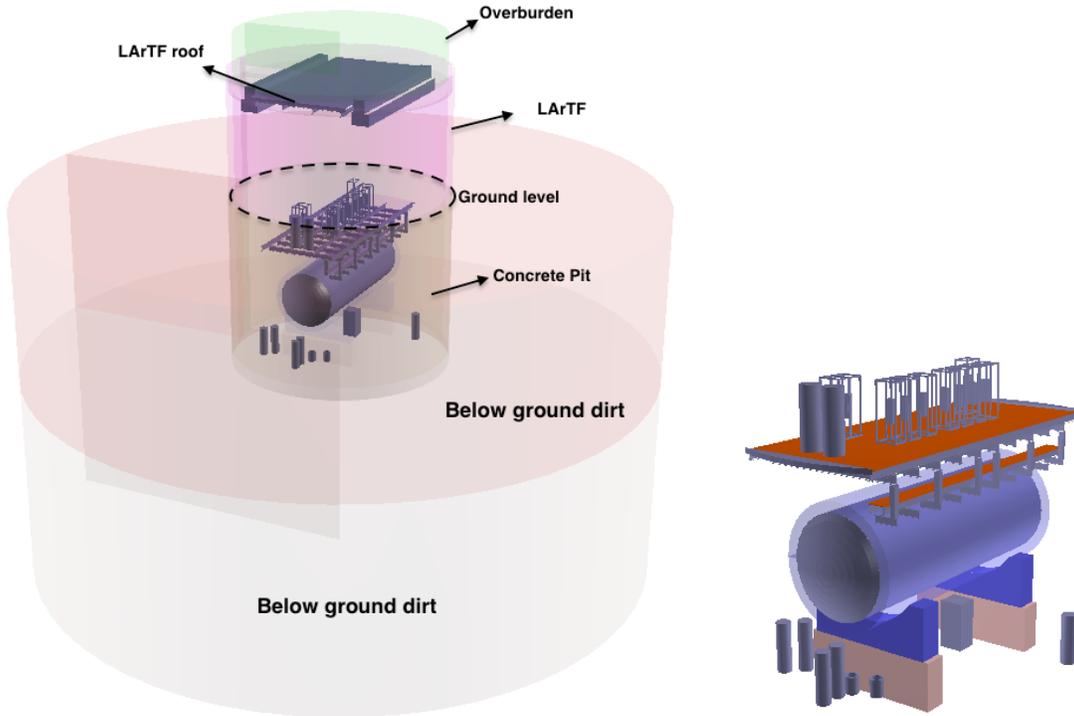
Figure 2: (Left) MicroBooNE geometry simulation of the detector and its surroundings. In order to clearly show the details of the simulation, a transparent view of the geometry is shown. The thick green, light-shaded cylinder located on the roof of the building shows the 3 m overburden under consideration. (Right) Zoomed-in view of the simulation of the material that is enclosed in the concrete pit of the LArTF building. Note that not all surrounding volumes are included in the simulation (e.g., cable tray, some extra racks and contents of racks), as shown in comparison with Figure 3.

the platform of the LArTF building.

One way to visualize the important features of the simulated geometry is to plot the stopping point positions of a set of simulated cosmic particles. Figure 4 shows the end-point distributions of all cosmic particles in YX (left) and YZ (right) projected planes of the MicroBooNE TPC without the overburden simulation. Figure 5 shows the same set of plots but with the 3 m overburden simulation. The figures clearly show most of the details of the simulated geometry. The MicroBooNE coordinate system is defined by Z in the neutrino beam direction, Y in the vertical direction, and X in the TPC drift direction. The origin of the coordinate system is on the upstream face of the MicroBooNE TPC in Y/Z and at the anode wire plane in X.

2.2 Cosmic ray generators

Two MC generators, CRY [6] and CORSIKA [7], are used to generate cosmic ray data samples and compared. These are described in Sections 2.2.1 and 2.2.2. Limitations of the
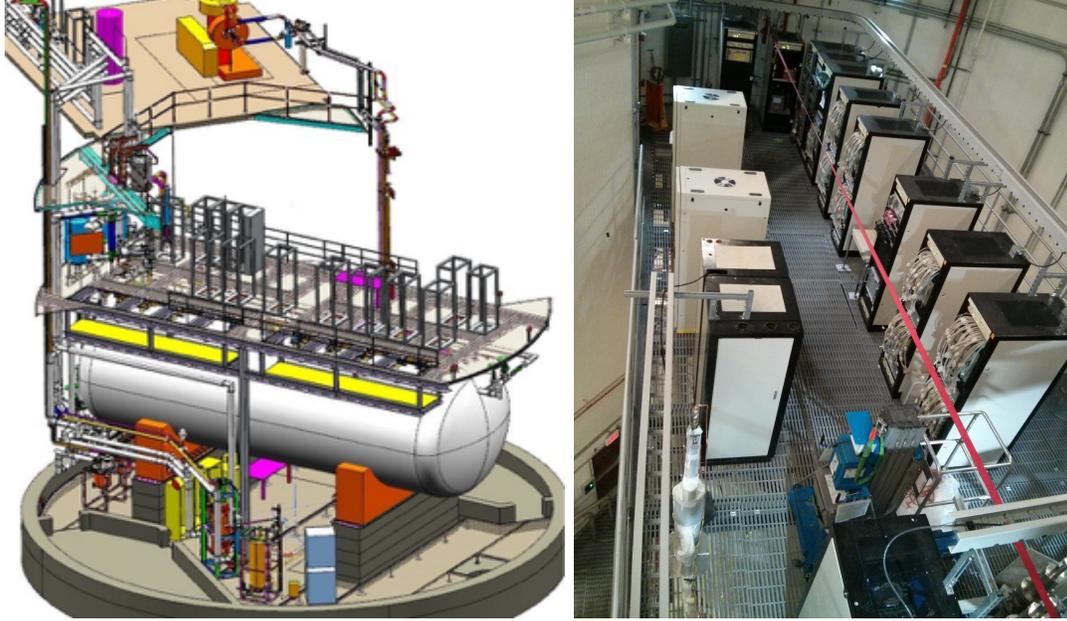
Figure 3: 3D drawing of the material surrounding the detector (left). Photograph of the actual material that currently exists on the platform of the LArTF building (right).
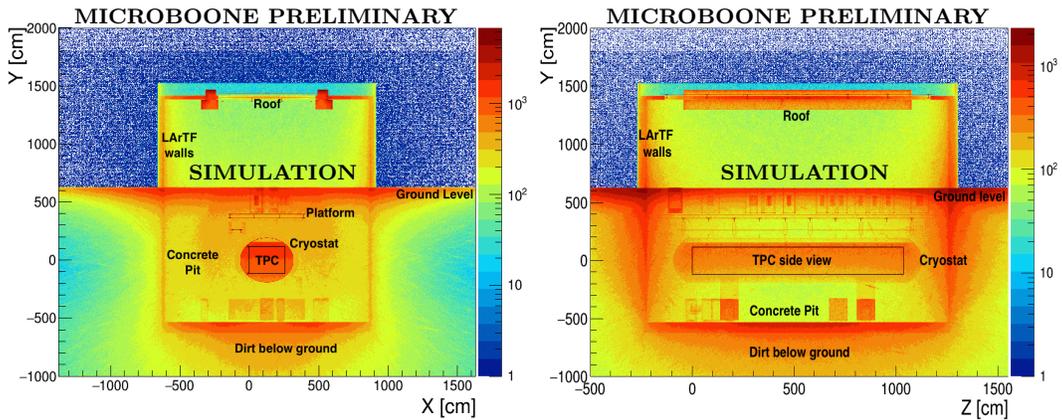

Figure 4: End point distribution of all cosmic particles using a data sample with no over-burden simulation in YX projection (left) and YZ projection (right) of the MicroBooNE geometry. Note that the particles are simulated starting at the plane y=18 m. The end points seen above y=18 m are particles that back scatter from the start point.

CRY generator software and a comparison of the flux from both generators are discussed, as CRY is predominantly used across many experiments. However, the results derived in this study are based on CORSIKA as it provides more detailed and accurate simulation of cosmic ray particle fluxes. The effect of flux model choices on cosmic ray particle rates is also presented. Also, note that throughout this document, the word *primary* is used as a descriptor for CRY/CORSIKA generated particles, and the word *secondary* refers to any particle produced by the CRY/CORSIKA "primaries" in their decays or interactions with
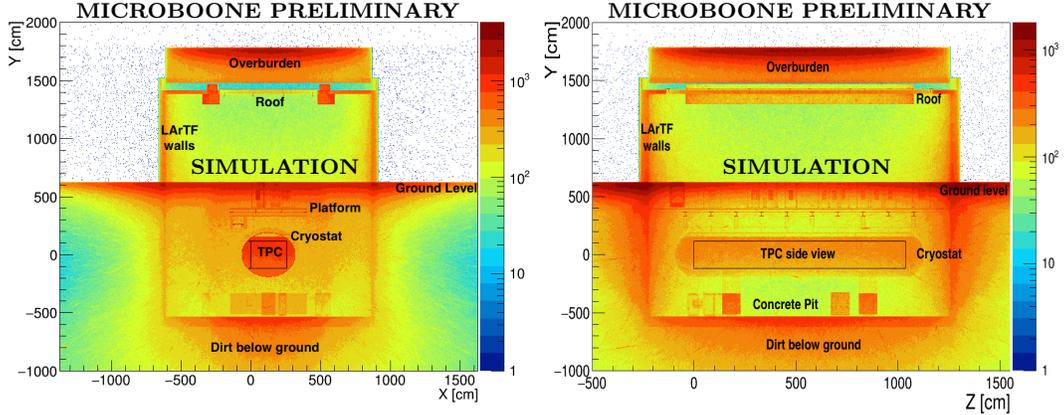
Figure 5: End point distribution of all cosmic particles using a data sample with 3 m concrete overburden simulation in YX projection (left) and YZ projection (right) of the MicroBooNE geometry. Note that the reason there are only few end points above ground and outside LArTF (compared to Fig. 4) is because the region above ground and outside LArTF is filled with vacuum in this sample. This is a minor difference and does not affect the conclusions presented in this study.

other materials.

2.2.1 CRY generator

The CRY MC generator is capable of generating all particle (and anti-particle) types at one of three altitudes: sea level, 2100 m, and 11300 m. CRY also provides a latitude dependent (no provision to specify longitude) geomagnetic cutoff of the primary cosmic-ray spectrum and modulation of the spectrum over time based on the average solar cycle. The latitude of 41.8^o N is currently set in CRY to compute a geomagnetic cutoff of the primary cosmic-ray spectrum. Although CRY allows one to input the date to set the current point in the solar cycle, the CRY interface in the LArSoft [8, 9] software framework (the *CRYHelper* class) always resets this to 1-1-2014.

Primary particle type	Absorption Length (gm/cm^2)	Sea level flux	226 m Level flux
Neutrons	148	1	1.20
Protons	110	1	1.28
Electrons	100	1	1.31
Muons	520	1	1.05

Table 1: Table of relative increases with respect to sea level flux. Increase in flux is shown for Fermilab altitude (226 m). L is the absorption length in terms of atmospheric density assuming average barometric pressure and temperature of 0 degree Celsius. Any energy dependence of absorption processes is ignored.
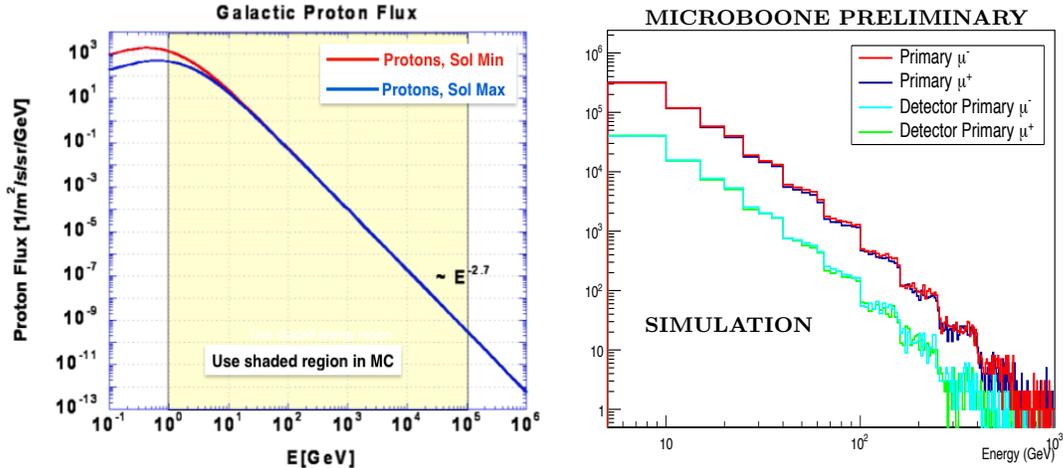
Figure 6: (Left) Energy spectrum of galactic protons incident on earth [6]. (Right) Muon energy spectra as generated by CRY.

There is no provision in CRY yet to specify an intermediate value between the three standard elevation points. Because of this, all MC samples generated with CRY for this work are at sea level. Following Equations (1) and (2) of Ref. [10], one can compute the relative increase in particle fluxes with respect to sea level to get an estimate of how flux varies with altitude (ignoring any energy dependence). Table 1 shows the anticipated increase in flux at 226 m for various particle types relative to sea level flux. One can see from the table that non-muon fluxes are significantly affected in going from sea level to Fermilab altitude.

CRY particle sampling is based on precomputed tables derived from a full MCNPX 2.5.0 [11] simulation which assumes *only* galactic protons in the incident flux spectrum. Figure 6 (left) shows the energy spectrum of galactic protons incident on Earth; only the highlighted region of the spectrum is used in the simulation. As will be seen from Section 2.3, the absence of non-proton nuclei in the incident flux severely underestimates the resulting hadron fluxes at all energies. Another known problem in CRY is that it uses large bin widths to store energy spectra, which results in inaccurate sampling of particle flux spectra. Figure 6 (right) shows the CRY generated energy spectra for μ^- and μ^+ demonstrating the step-like structure (especially above 40 GeV or so) due to large bin widths.

2.2.2 CORSIKA generator

The COsmic Ray SImulations for KAscade (CORSIKA) cosmic ray simulation package was used to validate and cross-check the cosmic ray particle fluxes predicted by CRY as it was deemed more reliable, accurate, and set as default. CORSIKA allows for the study of features not implemented in CRY, in particular:

- simulating multiple primary particle types other than protons

- simulating the particle fluxes at the Fermilab elevation (226 m)

7

- testing alternate models for cosmic shower evolution (e.g. FLUKA)

- simulating cosmogenic particle fluxes below 50 MeV

Also, unlike CRY, CORSIKA allows one to directly set the magnetic field components for a given geographic location. In the current CORSIKA simulation, the magnetic field components are currently set to Bx = 19.066 μT, Bz = 50.628 μT which are obtained from the NOAA [12] website by providing the Fermilab geographic location as input to their geomagnetic calculator. By adapting the work done by S. Tognini [13] in the NOνA collaboration, it was possible to quickly adapt CORSIKA output parsing and cosmic ray shower processing code to feed into LArSoft. CORSIKA version 7.4003 is used to generate a large sample of showers for various primary particle types.

There are a large number of configurable options available in CORSIKA. A subset of these options was explored and, in particular, the primary particle type, primary low energy cutoff, and low-energy hadronic interaction model were varied. The primary types include elementary particles and nuclei up to A=56. In order to compare with CRY, protons were chosen as well as a combination of elements to implement a multi-component model that will be discussed below. The primary low energy cutoff controls the lowest energy per nucleon and is typically around 1 GeV. Below 1 GeV the resulting shower particles have a low probability of reaching the surface. In ~1.0E6 showers, no proton showers that had particles reaching the surface with a primary kinetic energy below 1.4 GeV were found. The optimal value for this parameter depends on the altitude being considered. The low-energy hadronic interaction model is also configurable in CORSIKA. The two models studied are GHEISHA and FLUKA and will be discussed in Section 2.3.

The Constant Mass Composition model

To account for the diverse composition of primary particles impinging on the atmosphere, the Constant Mass Composition model (CMC) was used [14]. This model uses a parametrization of the spectra of a subset of primary components which are combined to reproduce the full primary particle spectrum. The CMC model does this using five components with a constant spectral index for each primary type: protons, He, N, Mg, and Fe. The flux of each primary type is specified using

$$\Phi_A(E) = K_A(E/1 \text{ GeV})^{-\gamma_A} \tag{1}$$

where A is the index of the primary type which varies over the subset of primary components p, He, N, Mg and Fe, E is the energy of the primary particle (per nucleon), K_A is the flux constant for primary type A, and γ_A is the spectral index of primary component type A. Table 2 lists the flux constant and spectral index for each primary type. These five component based parameterizations are provided as input to the CMC model.

In order to implement the CMC model within the CORSIKA framework it is necessary to run a sufficient number of showers of each primary type with the specified spectral index. The showers are then arranged into spills with the duration of 4 readout frames (6.4 ms)[1] at

---

[1]Note that during the 6.4 ms duration, the correlations between the primary particles would be lost

Components	K_A	γ
p	1.72×10^4	2.71
α	9.20×10^3	2.71
CNO	6.20×10^3	2.71
Mg	9.20×10^3	2.71
Fe	6.20×10^3	2.71

Table 2: Flux constants (K_A) and spectral indices (γ) for each primary component (denoted by A in Eq. 1) in the CMC model [14].

the surface, based on the specified flux constant for each primary type. The resulting lists of particles are then concatenated to form the total CMC model cosmogenic particle flux.

2.3 Flux model and generator comparisons

The dominant uncertainty in computing cosmogenic fluxes comes from the particle interaction models so it is important to consider the effects of model choices on the resulting secondary particle fluxes. Experimental data from BESS [15], indicates that FLUKA does a better job of modeling hadronic interactions at low energy, particularly for protons. CORSIKA can use the FLUKA 2011 model for hadronic interactions below 80 GeV, but, by default, GHEISHA is used and is built into the CORSIKA distribution. CORSIKA has to be pointed to the location of a working FLUKA installation in order to use the FLUKA model.

Figure 7 shows comparisons of the flux, for each simulated primary particle type, between CRY, CORSIKA-GHEISHA and CORSIKA-FLUKA models. In changing from the GHEISHA model to the FLUKA model in CORSIKA the fluxes of muons, electrons, and photons remain essentially unchanged. The neutron and proton flux, particularly below 1 GeV, is increased dramatically. The integrated neutron flux increases by a factor of 4.0 while the proton flux increases by a factor of 3.3. The CRY results are similar to those from the CORSIKA-GHEISHA model except that CORSIKA predicts a significant increase in the electromagnetic component. Also, CORSIKA does not exhibit the course binning effects that are present in CRY.

Figure 8 shows CORSIKA-FLUKA cosmogenic primary particle flux predictions at the top of the MicroBooNE TPC for both the proton-only and CMC primary models. In general the change from the proton only model to the CMC model increases the flux of each type of cosmogenic particle. Table 3 gives the predicted rate for each particle type along with the ratio of the rate relative to the CRY rate. The muon rate increases drastically, by 40%, when considering the CMC model. The neutron rates increase by a factor of 5.

---

due to the large acceptance of MicroBooNE (i.e., the showers that result from various primaries overlap in space/time). It is possible that there would be timing correlations in the secondaries induced by primaries but this has not been studied by the authors.
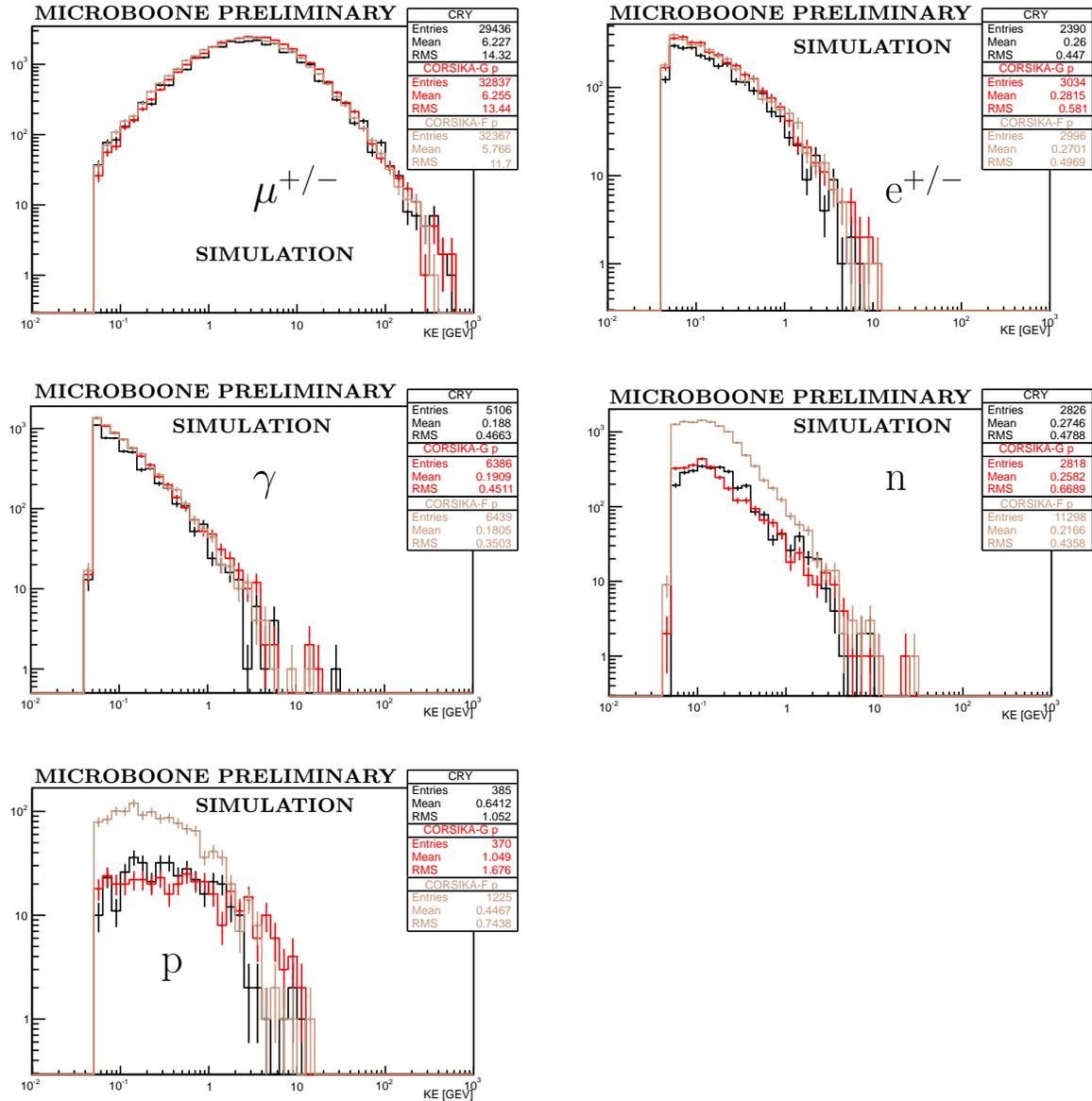
Figure 7: Comparisons of the energy distributions for each primary particle type through the top surface of the TPC active volume for CRY (black), CORSIKA-GHEISHA (red), and CORSIKA-FLUKA (tan). All three samples use only proton primaries and are made up of 2000 events that are 4.8 ms (3 read-out frames) long. Errors shown are statistical only. Note that in changing from the GHEISHA model to the FLUKA model in CORSIKA, the integrated neutron (proton) flux increases by a factor of 4.0 (3.3).

For the rest of this note, CORSIKA with CMC and FLUKA configuration represents our nominal simulation as it more accurately represents the expected cosmic ray particle fluxes. All conclusions derived in this note are based on this sample.
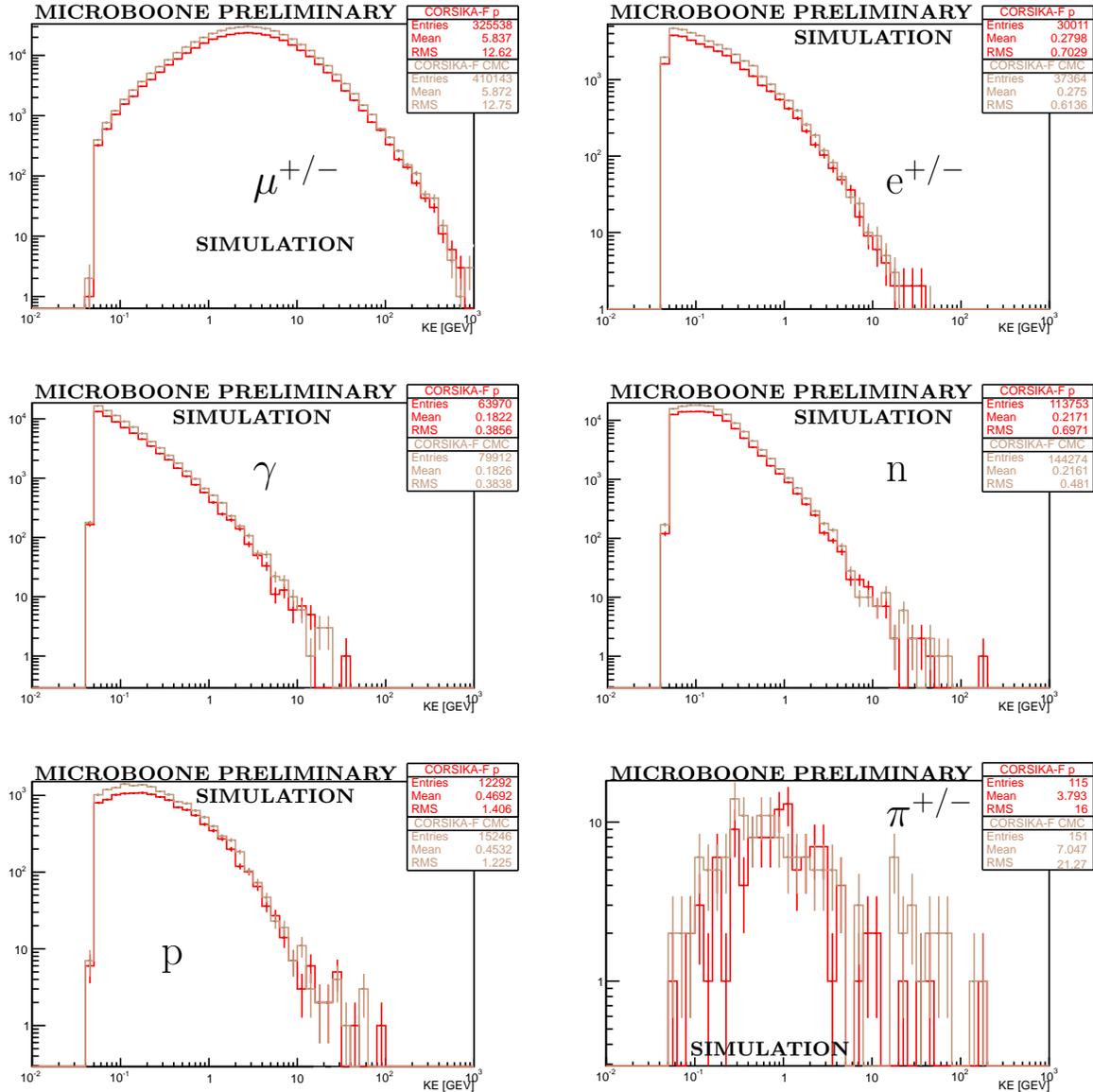
Figure 8: Comparisons of the energy distributions for each particle type through the top of the TPC active volume for CORSIKA-FLUKA with protons (red) and CORSIKA-FLUKA with the CMC Model (tan). The samples are made up of 19,982 events that are 4.8 ms (3 read-out frames) long.

3 Cosmogenic background rates

This section presents estimates of the sizes of various cosmogenic particles that enter the TPC using CRY and CORSIKA cosmic samples without an overburden present.

Primary particle	CRY Flux	CORSIKA GHEISHA Proton		CORSIKA FLUKA Proton		CORSIKA FLUKA CMC	
		Flux	Ratio	Flux	Ratio	Flux	Ratio
$\mu^{\pm}$	120.0 ± 0.2	128.7 ± 0.7	1.07 ± 0.01	127.7 ± 0.2	1.064 ± 0.002	160.9 ± 0.3	1.341 ± 0.003
$e^{\pm}$	12.4 ± 0.1	11.9 ± 0.2	0.96 ± 0.02	11.8 ± 0.1	0.95 ± 0.01	14.7 ± 0.1	1.18 ± 0.01
γ	25.8 ± 0.1	25.0 ± 0.3	0.97 ± 0.01	25.1 ± 0.1	0.97 ± 0.01	31.3 ± 0.1	1.21 ± 0.01
n	13.3 ± 0.1	11.0 ± 0.2	0.83 ± 0.02	44.6 ± 0.1	3.35 ± 0.03	56.6 ± 0.1	4.25 ± 0.03
p	1.92 ± 0.02	1.4 ± 0.1	0.73 ± 0.05	4.8 ± 0.04	2.50 ± 0.03	6.0 ± 0.1	3.13 ± 0.06
$\pi^{\pm}$	0.029 ± 0.003	0.067 ± 0.02	2.3 ± 0.7	0.045 ± 0.004	1.6 ± 0.2	0.059 ± 0.005	2.1 ± 0.3

Table 3: Table of fluxes, in $Hz \cdot m^{-2}$, for CRY and the various CORSIKA configurations. Ratios are given relative to the CRY rate. Both CRY and CORSIKA rates are given at the Fermilab elevation. Note that the CRY sea-level numbers are corrected for Fermilab elevation based on Table 1.

3.1 Analysis framework and data samples

The CRY and CORSIKA MC samples with and without overburden simulation are generated in LArSoft [8] version v04_14_00. Details about the overburden geometry can be found in Section 2.1. Each of the CRY samples has ∼40k generated events. An event here corresponds to a total generation time of 6.4 ms (the event time window is centered at the start of the drift window that encloses the beam gate). This broad generation time per event is required to accommodate cosmic tracks that occur at random times. The ∼40k event CRY samples correspond to 256 seconds in integrated beam spill time while the ∼20k event CORSIKA samples correspond to 128 secs.

In MicroBooNE, the total read-out time for a given event is three times (four times) the drift window for TPC (PMT) at 500 V/cm (3×1.6ms = 4.8 ms or equivalently 9600 time ticks with a sampling rate of 500 ns per tick). Although we are primarily interested in what happens in the drift window (1.6 ms), it is important to record information 1.6 ms before and after the event drift window in order to accommodate cosmic ray tracks that are not fully contained within the neutrino event drift window [4]. Note that currently MicroBooNE is running at an electric field of 273 V/cm which results in a drift time of ∼2.3 ms for an electron to travel the full distance (2.56 m) between cathode and anode.

At many places in the following sections, the event rates are quoted for 211 seconds or equivalently 1.32×10^8 neutrino beam spills (a BNB beam spill window corresponds to 1.6 μs). The significance of 211 seconds is that it corresponds to the total beam exposure time for a BNB run with 6.6×10^{20} POT, assuming 5×10^{12} POT per spill. This assumes 100% rejection of out-of-spill cosmogenic events based on PMT timing information.

3.2 Overall particle rates

Table 4 shows the simulated number of cosmic particles that enter the TPC active volume in a 1.6 ms time window. A minimum energy cut of 100 MeV is applied to electrons and photons to remove very low-energy particles which are of little interest for this study. The CORSIKA-CMC-FLUKA model represents the nominal simulation. For comparison,

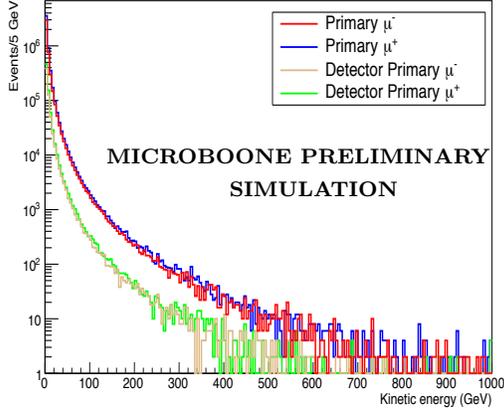| Particle type	CRY PROTON	CORSIKA CMC GHEISHA	CORSIKA PROTON FLUKA	CORSIKA CMC FLUKA
μ^-	3.079±0.004	4.22±0.02	3.093±0.006	4.006±0.007
μ^+	3.249±0.004	4.91±0.02	3.895±0.007	4.810±0.008
neutron	4.919±0.005	5.99±0.03	10.75±0.01	13.77±0.01
proton	0.447±0.001	0.54±0.01	0.969±0.004	1.245±0.004
γ (>100 MeV)	0.613±0.002	0.71±0.01	0.524±0.003	0.657±0.003
e^- (>100 MeV)	1.178±0.002	1.36±0.01	1.004±0.004	1.260±0.004
e^+ (>100 MeV)	0.335±0.001	0.37±0.01	0.280±0.002	0.347±0.002

Table 4: Number of primary plus secondary particles expected in the TPC active volume per 1.6 ms time window for various particle types. In this case, the geometry simulation doesn't include any type of overburden. Both CRY and CORSIKA numbers correspond to Fermilab altitude (note that CRY numbers are corrected for Fermilab altitude based on Table 1).

estimates from CRY and other CORSIKA configurations are also shown. All numbers correspond to Fermilab elevation. Table 4 shows that muons and neutrons make up the majority of the background.
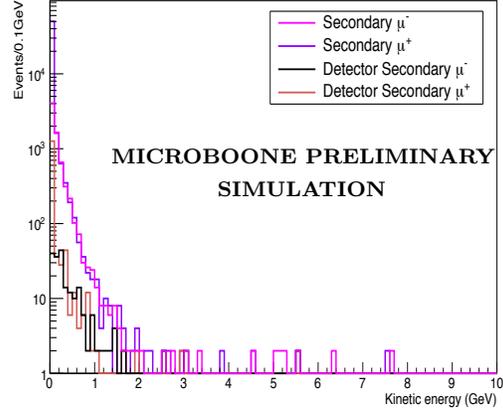
Figures 9 and 10 shows the kinetic energy distribution of important cosmic backgrounds predicted by the nominal simulation (CORSIKA-CMC-FLUKA). As expected, most of the primary muons reach the detector and there is not much secondary muon production (Figures 9a and 9b). A large number of primary neutrons with kinetic energies between 0.1 and 4 GeV manage to reach the detector (see Fig. 9c). A lot of secondary neutrons are produced due to interactions of primary particles within and outside the detector as shown in Figure 9d. Although small compared to neutrons, the primary proton background rate is significant (Fig. 9c) and the secondary proton production is comparable to neutrons (Fig. 9d).

It is interesting to note from Figures 10a and 10c that a small (but significant) number of primary photons and a negligible number of primary electrons/positrons with energies greater than 100 MeV reach the detector. This lower rate is due to the large amount of absorptive material surrounding the detector, including the inactive argon in the cryostat. Figure 11 shows how the primary photons are stopped in the surrounding volume of the TPC, especially in the liquid argon volume that surrounds the detector. This is due to the short conversion length of photons (18 cm) in liquid argon [17, 18]. Figure 12 shows the start point distribution of all secondary photons with energies above 100 MeV that enter the active volume of the TPC. Most secondary photons are produced inside and in the walls of the cryostat.
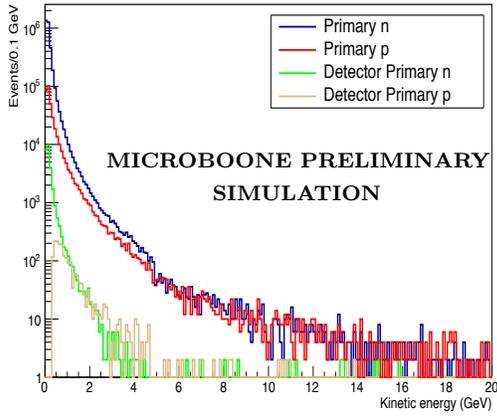
The secondary electron and photon backgrounds as shown in Figures 10b and 10d are mainly produced by muons through δ rays. It is this background that is worrisome for single e/γ searches. Also equally worrisome are the e/γ backgrounds induced by primary photons and hadrons. The next part of this section shows a detailed study of these backgrounds.
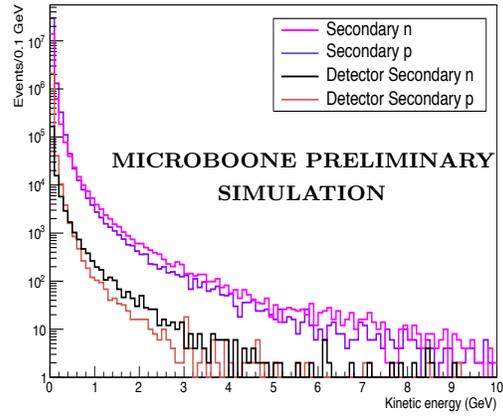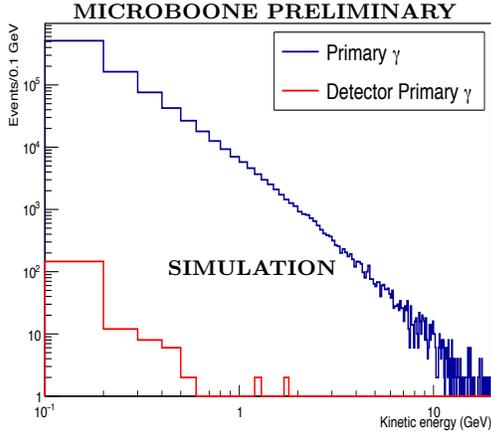
(a) Primary muons

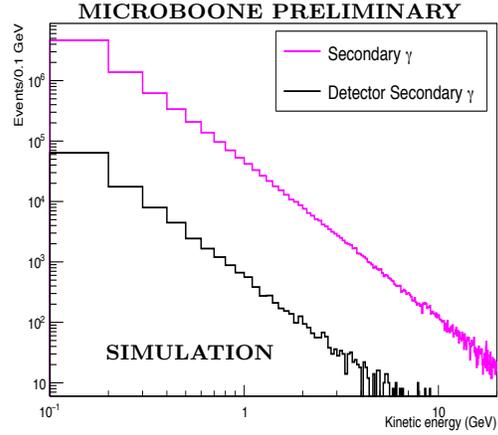(b) Secondary muons

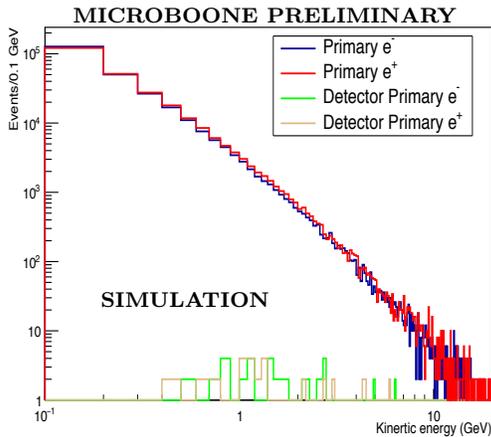(c) Primary neutrons and protons

(d) Secondary neutrons and protons

Figure 9: Kinetic energy distributions of muons, protons, and neutrons using the CORSIKA-CMC-FLUKA sample without any overburden simulation. Plots also show the kinetic energy distributions of particles that enter the TPC active volume (referred to as "detector primary" or "detector secondary" in the plots). These plots correspond to a total of 256 seconds in integrated beam spill time. Please note the difference in axes scales between the plots.
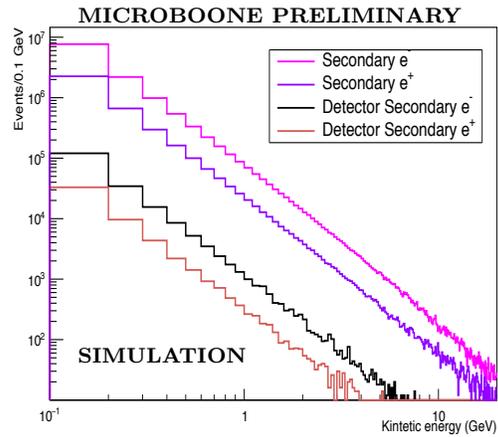
(a) primary photons

(b) secondary photons

(c) Primary electrons

(d) Secondary electrons

Figure 10: Kinetic energy distributions of electrons and photons using the CORSIKA-CMC-FLUKA sample without any overburden simulation. Plots also show the kinetic energy distributions of particles that enter the TPC active volume (referred to as "detector primary" or "detector secondary" in the plots). The photon and electron plots include an energy cut of 100 MeV. These plots correspond to a total of 256 seconds in integrated beam spill time. Please note the difference in axes scales between the plots.

3.3 Cosmogenic shower backgrounds

Cosmic events that induce EM showers inside the active volume of the detector can potentially form a significant background to ν_e appearance and single-photon searches. EM showers are mainly induced by primary muons that enter the detector volume or pass close to the walls of the detector. In this note, cosmogenic shower backgrounds are defined as follows:

- electrons created in the TPC active volume by a Compton scatter which are candidate "electron-like" showers, and are therefore candidate backgrounds primarily to ν_e and single-electron low energy searches

- an e^+/e^- pair created in the TPC active volume by the photon pair production process which are candidate "photon-like" showers, and are therefore candidate backgrounds primarily to single-photon low energy searches.

There are two main processes that produce the parent photon of these backgrounds. The dominant process is a muon which produces a delta-ray which in turn creates a photon through bremsstrahlung. A muon can also create a photon through bremsstrahlung directly. The latter process results in about 3% of these events.

In addition to muon induced photons, a high energy primary photon that passes close to the detector walls can induce an EM shower via pair-production or Compton scattering process. This rate is found to be non-negligible. The background showers are also produced in significant quantities by other primary particles, such as neutrons, protons, and pions. Table 5 shows cosmogenic background shower counts expected from a BNB exposure of 211
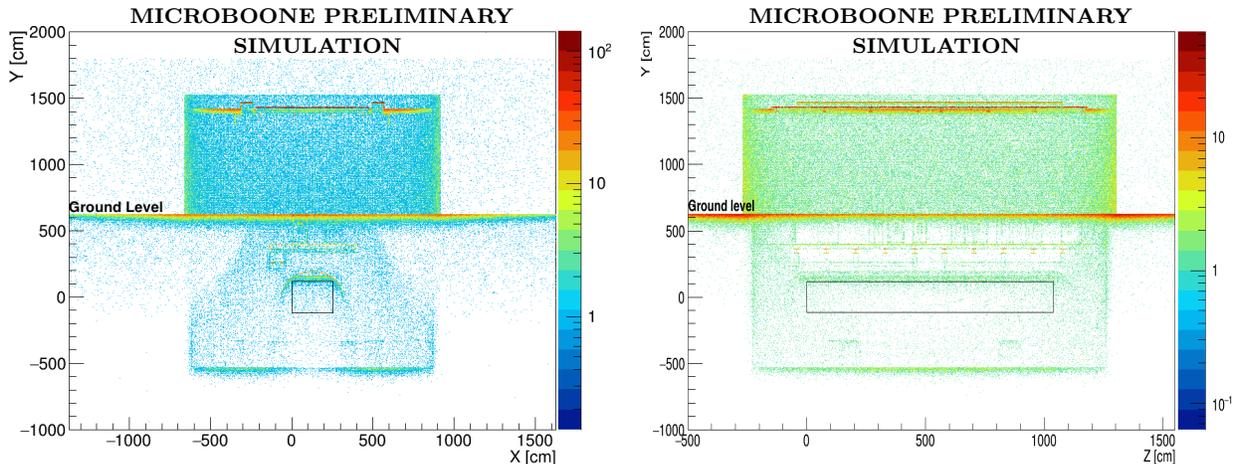

Figure 11: End point distribution of primary photons with energies above 100 MeV in the YX (left) and YZ (right) projection of the MicroBooNE TPC. The end point for photons is defined as the point where it converts. These distributions are obtained using a cosmic data sample with no overburden simulation. Note that the particles are simulated starting at the plane y=18 m.
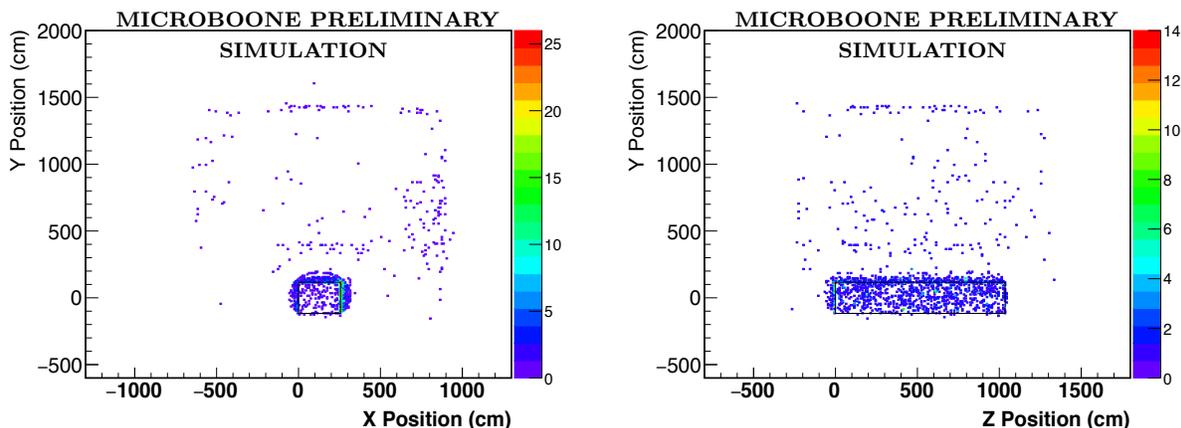
Figure 12: Start point distribution of all secondary photons with energies above 100 MeV that enter the detector in the YX (left) and YZ (right) projection of the MicroBooNE TPC using a data sample with no overburden simulation.

Process (in spill)	Source (Primary particle)	CRY PROTON	CORSIKA CMC GHEISHA	CORSIKA PROTON FLUKA	CORSIKA CMC FLUKA
Compton	μ in AV	190±11	297±70	249±20	318±23
Pair production	μ in AV	12220±90	18225±549	13369±150	15917±162
Compton	μ not in AV	4	0	0	3
Pair production	μ not in AV	144±10	33±23	29±7	71±11
Compton	γ	1.3±0.9	0	3.4±2.4	3.3±2.3
Pair production	γ	110±9	264±66	217±19	231±20
Compton	not a μ or γ	12±3	17±17	15±5	28±7
Pair production	not a μ or γ	640±21	1550±160	1222±45	1474±49
Expected beam-related "electron-like" background [5]	~450				
Low energy excess signal [1]	~100				
$\nu_\mu \to \nu_e$ oscillation signal (Δm^2=0.43 eV^2, sin$^2 2\theta_{\mu e}$=0.013) [16]	~70				

Table 5: Cosmogenic background showers occurring in the fiducial volume without overburden classified according to the shower-inducing interaction process (compton or pair production). Energy of the initiating photon is required to be greater than 200 MeV. Event counts correspond to a total of 211 seconds in integrated beam spill time. For comparison, a sample $\nu_\mu \to \nu_e$ sterile neutrino oscillation signal expected for the same exposure is also shown corresponding to the best-fit parameters from the Kopp *et al.* analysis [16] of Δm^2=0.43 eV^2, sin$^2 2\theta_{\mu e}$=0.013. Also shown for comparison is a scaled "electron-like" low energy excess signal from MiniBooNE [1]. *AV* here stands for active volume of the detector. Note that the cosmogenic background shower counts shown in the table are not exclusively single-shower cosmogenic events; multi-shower events are included. The beam-related background and signal predictions show the overall scale of reconstructed events for 6.6×10^{20} POT (i.e., unlike cosmogenic background numbers, they include an assumed reconstruction efficiency, e.g., 80% and other topological cuts) and include an energy cut of 200 MeV on the reconstructed neutrino energy.

17

Process (in spill)	Source (primary particle)	CORSIKA CMC GHEISHA	CORSIKA CMC FLUKA
Compton	μ in AV	1337±149	1401±48
Pair production	μ in AV	46669±878	40645±260
Compton	μ not in AV	0	5
Pair production	μ not in AV	149±50	192±18
Compton	γ	17±17	33±7
Pair production	γ	890±120	780±40
Compton	not a μ or γ	83±37	108±13
Pair production	not a μ or γ	3620±240	3430±75

Table 6: Cosmogenic background showers occurring in the fiducial volume without overburden classified according to the shower-inducing interaction process (compton or pair production). Energy of the initiating photon is required to be greater than 100 MeV. Event counts correspond to a total of 211 seconds in integrated beam spill time. *AV* here stands for active volume of the detector. Note that the shower counts shown in the table are not exclusively single-shower cosmogenic events; multi-shower events are included.

seconds. Shower counts shown in the table require that the photon interaction which initiates the EM shower occur in the fiducial volume of the detector, defined as 30 cm downstream and 100 cm upstream of the TPC boundaries in the Z direction (long direction, collinear with the beam) and 25 cm from all other walls of the TPC. Initiating photon energy is required to be 200 MeV in Table 5 (100 MeV in Table 6). In a Compton scatter, the daughter electron is also required to have an energy greater than 200 MeV in Table 5 (100 MeV in Table 6). As can be seen from the tables, the largest background comes from muon induced photons converting to e^+/e^- pairs.

The listed backgrounds in Table 5 are sub-divided according to each photon's matching primary particle. If the primary particle is a muon, a distinction is made as to whether it intersects the TPC active volume boundaries or not. Classifying backgrounds this way provides crucial information as to whether cuts can be applied to reduce these background events. Figure 13 (left) shows the energy distribution of background shower events with E>10 MeV. The energy of these background events lie in the region of interest of MicroBooNE physics. An overburden will have little effect on the rate of primary muons, the majority of which will enter the detector and act as dominant source of shower backgrounds. So, it is very important to devise a set of cuts to reduce this background in order to successfully perform searches involving single electrons or photons.

The background showers shown in Table 5 can be divided into what might be *taggable* or *untaggable*[2] background. A shower background is considered untaggable if the photon that initiates the shower is created outside the TPC active volume, or its lineage, traced back to the particle that enters the TPC active volume, must be composed entirely of neutral particles. Additionally, if the associated primary cosmic particle is a muon, it must not enter the active volume. The right hand side plot in Figure 13 shows the shower energy distri-

---

[2]Please note that in principle further reduction is possible for the "'untaggable" shower category, but the definition adopted in the note is a much more general definition for signal events *i.e.,* if one defines the signal topology as a single shower in the TPC active volume.
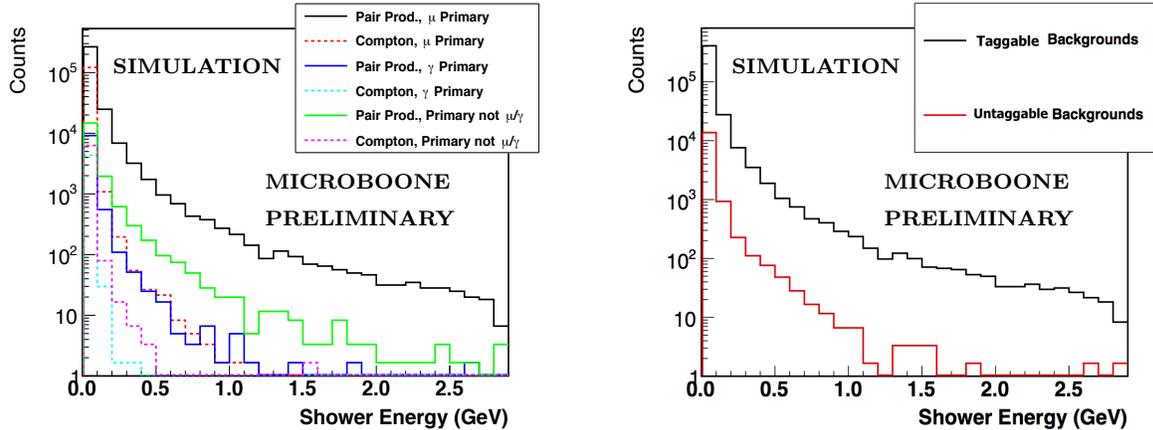
Figure 13: Energy distribution of cosmogenic background showers (E>10 MeV) occurring in the detector fiducial volume (defined in the text) using the CORSIKA-CMC-FLUKA sample without overburden. Showers are sub-divided according to their matching primary particle (left) and whether they are taggable or not (right). Note that for showers above 200 MeV, 33% (52%) of the taggable (untaggable) background is single-shower background. Event counts shown in the figure correspond to a total of 211 seconds in integrated beam spill time.

bution of these backgrounds for E>10 MeV. MicroBooNE has studied strategies to mitigate the taggable backgrounds [5]. One of the important cuts devised to reduce the muon induced shower background is the *muon cylinder cut* which identifies and removes background showers that originate close to a muon track. Non-muon induced showers (which are mostly pair-produced) are more challenging to remove; a combination of dE/dx and other cuts like backward distance to wall (BDtoW) or backward distance to top wall (BDtoTopW) [5] are devised to reduce this background. Although the mitigation studies demonstrated good cosmic shower rejection efficiency, it should be noted that they are performed with truth-based information and assume a flat 94% efficiency in identifying pair-produced showers based on dE/dx. This rejection efficiency needs to be demonstrated on data.

In the case of non-muon and non-photon induced shower background (see rows 7 and 8 of Table 5), the mechanism through which showers are generated is usually a hadronic interaction that creates a neutral pion which then decays into a photon producing showers. Table 7 shows the particle types of non-muon or non-photon primaries that are ancestors of a shower background. Primary protons and neutrons contribute much more than other primaries in creating these background showers. Figure 14 shows the number of cosmogenic background showers as a function of the energy of their matching non-muon or non-photon ancestor. It is interesting to note that some of these hadronic showers create multiple background showers[3] in the TPC active volume, see Figure 15. Out of the total non-muon or

---

[3]Such large energy depositions in the detector and multiple showers pointing to the same origin should provide an identifiable background signature and could potentially be removed. Note that no attempt is

non-photon induced shower background, 22% of it is single-shower background. To understand the effect of cosmogenic showers on the sensitivity to an electron-like or photon-like signal[4], it is useful to compare rows 5 to 8 of Table 5 to the intrinsic background and signal predictions provided in the same Table. From that comparison, it is clear that non-muon induced cosmogenic background showers will present a challenge to at least single-photon searches in MicroBooNE, and contribute non-negligibly as background to the single-electron

made to reject these multiple shower events in this study.

[4]Note that while the low energy excess signal estimate provided in Table 5 is not explicitly a signal prediction for a photon-like excess, it is still instructive since a photon-like excess is expected to be of the same order for most underlying excess scenarios.

Ancestor particle type	No. of cosmogenic shower events
$\bar{p}$	61
π^-	184
e^+	56
e^-	83
π^+	138
p	685
n	295

Table 7: Particle types of non-muon or non-photon primaries that are ancestors of a cosmogenic background shower (corresponds to rows 7 and 8 in Table 5) using the CORSIKA-CMC-FLUKA sample without overburden. Event counts correspond to a total of 211 seconds in integrated beam spill time.
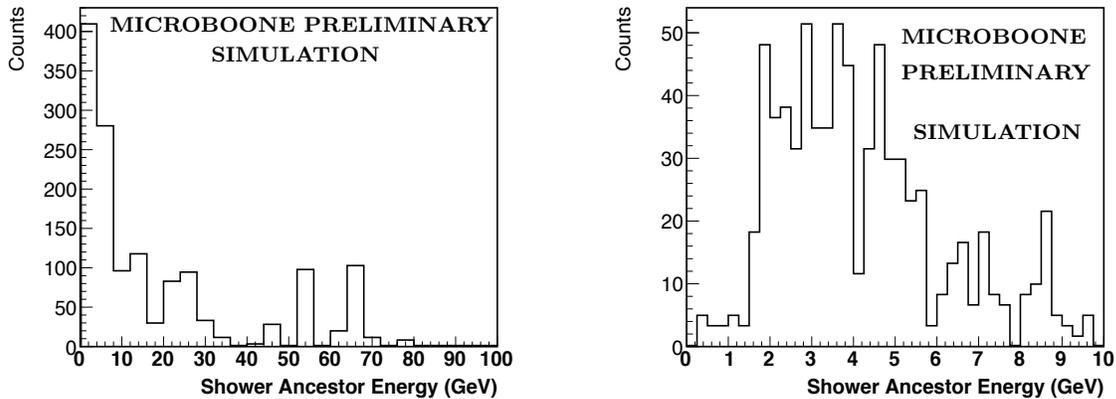

Figure 14: (Left) Number of cosmogenic background showers as a function of the energy of their matching non-muon or non-photon ancestor. Notice the really high energy ancestors that can result in a large number of showers. (Right) Zoomed-in view of the plot on the left for the energy range 0 to 10 GeV. Event counts in both figures correspond to a total of 211 seconds in integrated beam spill time.
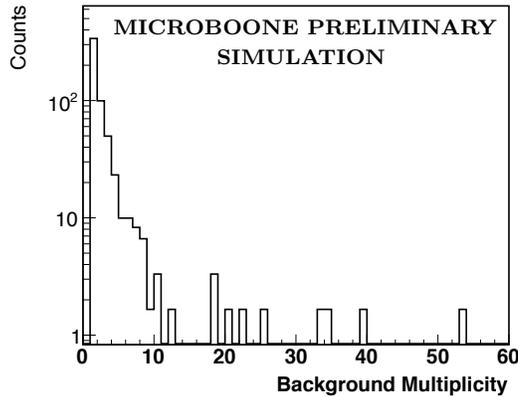
20

Figure 15:   Shower multiplicity for non-muon and non-photon primaries. Event counts correspond to a total of 211 seconds in integrated beam spill time.
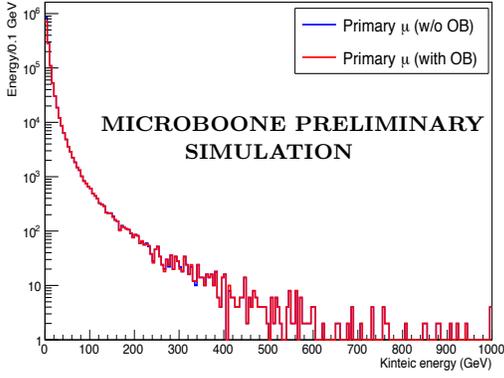
searches.

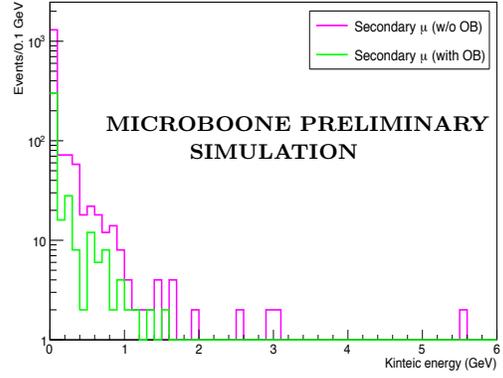# 4   Simulated background rates with overburden

In this section, the effect of a three meter concrete overburden on various particle rates is shown. The overburden is located on the LArTF roof as a solid concrete disc with a diameter matching the experimental pit. Given the position of the overburden in the MicroBooNE geometry, an overburden will *primarily* reduce the primary (or atmospheric) particle rates. Some particles back scatter from the geometry below and enter the volume of the overburden but this rate is found to have no effect on the final results. In particular, the primary motivation to install an overburden is to reduce non-muon primaries (such as neutrons and e/γ primaries) as muons are nearly unaffected by concrete. The original motivation for the overburden was to remove shower backgrounds induced by primary cosmogenic photons. However, as demonstrated in Section 3 (Figs. 9 and 10) and below, the secondary shower backgrounds induced by primary hadrons are several times larger than those induced by primary photons. The reduction of these latter backgrounds achieved with the overburden is therefore also of particular importance.

Table 8 shows the effect of overburden on primary and secondary backgrounds that enter the active volume of the detector. Rates shown in the table correspond to 211 seconds of integrated beam spill time. The biggest effect of overburden is on primary neutrons, protons, electrons and photons, reducing them by about 75%, 92%, 100% and 80% respectively. As expected, primary muons are mildly affected by the concrete overburden (reduced by about 9%).
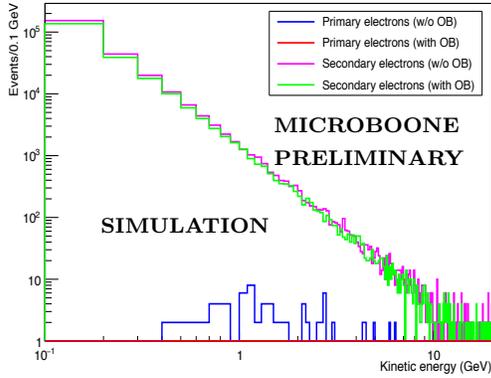
Table 8 also shows the indirect effect of an overburden on secondary particle rates. In particular, secondary neutron and proton production is reduced significantly ($\sim$62% to $\sim$72%)
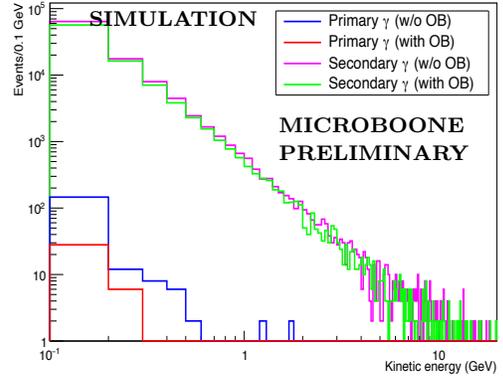
21

(a) Primary Muons

(b) Secondary Muons

(c) Electrons

(d) Photons

(e) Neutrons

(f) Protons

Figure 16: Energy distribution of various cosmic particles that enter the TPC with and without overburden simulation using the CORSIKA-CMC-FLUKA sample. Particles coming from primary (CORSIKA generator output) and secondary (Geant4) processes are separated to show the effect of overburden separately. In the case of muons, photons and electrons, a 100 MeV cut is implemented. Rates shown correspond to 256 seconds of integrated beam spill time. In the plots, *OB* is used as a short form for overburden. Please note the difference in axes scales between the plots.

Particle	Primary Particle rate		Fractional	Secondary Particle rate		Fractional
type	(w/o OB)	(with OB)	reduction (%)	(w/o OB)	(with OB)	reduction (%)
μ^-	528154±935	478276±890	9.4±0.2	169±17	60±10	60±10
μ^+	633114±1024	573600±975	9.4±0.2	1176±44	267±21	77±5
neutron	21879±190	5277±94	75±1	1793492±1724	676482±1059	62.3±0.1
proton	1581±51	129±15	92±4	162642±519	45747±275	71.9±0.4
γ (>100 MeV)	147±16	28±7	80±20	86527±379	77256±358	10.7±0.6
e^- (>100 MeV)	33±7	0	100	166126±525	150753±500	9.3±0.4
$e+$ (>100 MeV)	27±7	0	100	45780±275	38403±252	16.1±0.8

Table 8: Primary and secondary particle rates expected in the TPC active volume for various particle types with and without overburden (OB) using the CORSIKA-CMC-FLUKA sample. Rates shown correspond to 211 seconds of integrated beam spill time.

due to the reduction in the primary neutron background. Most of the secondary electromagnetic background seen in the table is induced by primary muons. With the inclusion of the overburden, these rates are reduced by about ∼9% to ∼16% due to the reduction of primary muons. Figure 16 shows the energy distribution of various backgrounds (both primary and secondary) that enter the active volume of the detector with and without overburden using the nominal sample.

In Sections 4.1 and 4.2 we explore the effect of the overburden on the MicroBooNE electromagnetic excess search. Specifically, the following question is addressed: How does an overburden affect the cosmogenic shower background in particular untaggable shower background? In other words, we want to verify that the secondary production in the overburden doesn't significantly increase this background.

4.1 Effect of overburden on cosmogenic shower backgrounds

In order to see the effect of an overburden on cosmogenic shower backgrounds, the analysis shown in Section 3.3 is repeated with the overburden cosmic sample. Table 9 shows how the background shower counts vary with the inclusion of overburden (compare columns 3 and 4 in the table). Initiating photon energy is required to be 200 MeV in Table 9 (100 MeV in Table 10). In a compton scatter, the daughter electron is also required to have an energy greater than 200 MeV in Table 9 (100 MeV in Table 10). Column 5 in the table shows the fractional reduction due to overburden. As expected, the overburden causes large reductions in non-muon induced backgrounds and modest reductions to muon-induced backgrounds. This result shows that the overburden configuration does not increase the cosmogenic background shower rate, and furthermore the non-muon-induced background is significantly reduced. Figure 17 (left) shows the energy distribution of background shower events (E>10 MeV) in Table 9.

Table 11 categorizes the electron-like (Compton) and photon-like (pair production) showers shown in Table 9 into taggable and untaggable backgrounds (see Section 3.3). The overburden gives an overall reduction of 83% (6%) in the case of untaggable (taggable) shower background. It is evident from this that the motivation for overburden is stronger for the single-photon excess search. The next section studies what portion of the total shower background is directly induced by the overburden.

Process (in spill)	Source (primary particle)	Shower counts (w/o overburden)	Shower counts (with overburden)	Fractional reduction (%)
Compton	μ in AV	318±23	265±21	20±10
Pair production	μ in AV	15917±162	15539±161	2±1
Compton	μ not in AV	3	0	100
Pair production	μ not in AV	71±11	28±7	60±20
Compton	γ	3.3	0	100
Pair production	γ	231±20	6.6	97±12
Compton	not a μ or γ	28±7	1.7	90±30
Pair production	not a μ or γ	1474±49	244±20	83±5
Expected beam-related "electron-like" background [5]		$\sim$450		
Low energy excess signal [1]		$\sim$100		
$\nu_\mu \to \nu_e$ oscillation signal (Δm^2=0.43 eV^2, $\sin^2 2\theta_{\mu e}$=0.013) [16]		$\sim$70		

Table 9: Cosmogenic background showers occurring in the fiducial volume (as defined in Section 3.3) with and without overburden classified according to the shower-inducing interaction process (compton or pair production). Energy of the initiating photon is required to be greater than 200 MeV. Event counts correspond to a total of 211 seconds in integrated beam spill time. For comparison, a sample $\nu_\mu \to \nu_e$ oscillation signal expected for the same exposure is also shown corresponding to the best-fit parameters from the Kopp *et al.* analysis [16] of Δm^2=0.43 eV^2, $\sin^2 2\theta_{\mu e}$=0.013. Also shown for comparison is the estimated "electron-like" low energy excess signal [1]. *AV* here stands for active volume of the detector. Note that the cosmogenic background shower counts shown in the table are not exclusively single-shower cosmogenic events; multi-shower events are included. The beam-related background and signal predictions show the overall scale of reconstructed events for 6.6×10^{20} POT (i.e., unlike cosmogenic background numbers, they include an assumed reconstruction efficiency, e.g., 80% and other topological cuts) and include an energy cut of 200 MeV on the reconstructed neutrino energy.

Process (in spill)	Source primary particle	Shower counts (w/o overburden)	Shower counts (with overburden)	Fractional reduction (%)
Compton	μ in AV	1401±48	1274±46	9±5
Pair production	μ in AV	40645±260	39013±254	4±1
Compton	μ not in AV	5	1.7±1.7	66±34
Pair production	μ not in AV	192±18	95±13	50±10
Compton	γ	33±7	0	100±30
Pair production	γ	780±40	61±10	92±7
Compton	not a μ or γ	108±13	23±6	79±16
Pair Production	not a μ or γ	3430±75	585±31	83±3

Table 10: Cosmogenic background showers occurring in the fiducial volume (as defined in Section 3.3) with and without overburden classified according to the shower-inducing interaction process (compton or pair production). Energy of the initiating photon is required to be greater than 100 MeV. *AV* here stands for active volume of the detector. Event counts correspond to a total of 211 seconds in integrated beam spill time. Note that the shower counts shown in the table are not exclusively single-shower cosmogenic events; multi-shower events are also included.
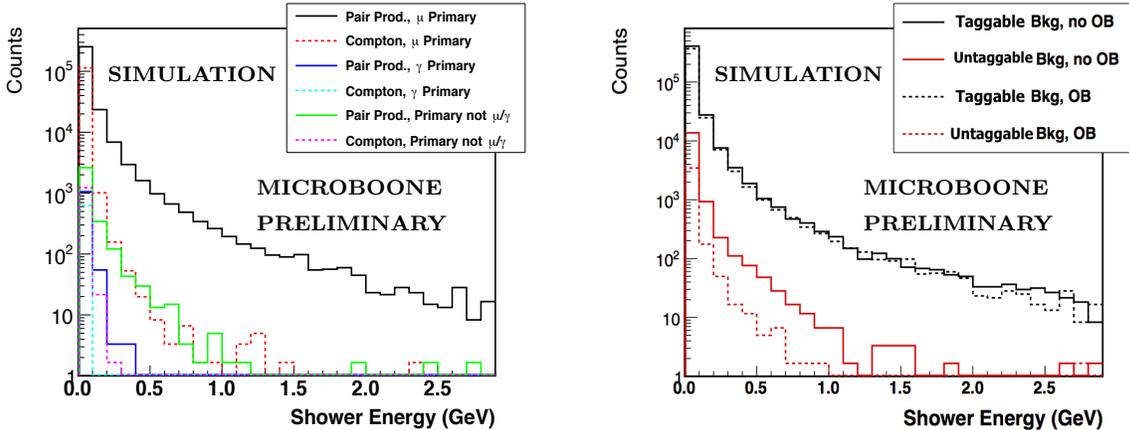
Figure 17: Energy distribution of cosmogenic background showers (E>10 MeV) occurring in the detector fiducial volume (defined in the text) using the CORSIKA-CMC-FLUKA sample with 3 m concrete overburden. Showers are sub-divided according to their matching primary particle (left) and whether they are taggable or not (right). Event counts corresponds to a total of 211 seconds in integrated beam spill time. In the right-hand side plot, *OB* is used as a short form for overburden. Note that for shower energies greater than 200 MeV, 33% (52%) of the taggable (untaggable) background is single-shower background in the case of no overburden. In the case of 3 m overburden, 33% (44%) of the taggable (untaggable) background is single-shower background.

4.2   Secondary production in the overburden

The concrete overburden is located ∼14 meters from the top surface of the MicroBooNE detector. A large amount of absorptive material surrounds the detector in this gap, such as the walls, platform, electronics racks, cryogenic piping and the passive portions of the cryostat. Any secondary production due to interactions in the overburden would need to survive all this material before it can reach the detector. Also, the overburden itself has a thickness of 3 m which makes it possible to re-absorb most of the background that it creates.

In order to understand how these features affect particle propagation, the end point distribution of all particles that are created in the overburden is plotted. Figure 18 shows this distribution in the YX (left) and YZ (right) projection of the detector. Most of the background created in the overburden gets re-absorbed in the overburden and for most of what is left, the surrounding material does a good job of absorbing it. One can see from the figure that only a little of this background reaches the detector. Figure 19 shows the same set of plots (as in Figure 18) but with an energy cut of 100 MeV which further suppresses this background. Figure 20 shows the start point distribution of all secondary photons with energies above 100 MeV that enter the detector (compare to Figure 12). Only a negligible fraction of those photons originate in the overburden.

The shower background that originates from interactions in the overburden is also cal-

25

Process (in spill)	Background type	Shower counts (w/o overburden)	Shower counts (with overburden)	Fractional reduction (%)
Compton	Untaggable	8.2±3.7	0	100
Pair production	Untaggable	547±30	98±13	82±3
Compton	Taggable	345±24	267±21	23±8
Pair production	Taggable	17146±168	15720±161	8±1
Expected beam-related "electron-like" background [5]		~450		
Low energy excess signal [1]		~100		
$\nu_\mu \to \nu_e$ oscillation signal (Δm^2=0.43 eV^2, $\sin^2 2\theta_{\mu e}$=0.013) [16]		~70		

Table 11: Cosmogenic background showers occurring in the fiducial volume (as defined in Section 3.3) with and without overburden classified according to the shower-inducing interaction process (compton or pair production). Energy of the initiating photon is required to be greater than 200 MeV. The electron-like (compton) and photon-like (pair production) showers are further divided based on whether they are taggable or not following the definition in Section 3.3. Note that in the case of no overburden, 33% (52%) of the taggable (untaggable) background is single-shower background. In the case of 3 m overburden, 33% (44%) of the taggable (untaggable) background is single-shower background. Event counts correspond to a total of 211 seconds in integrated beam spill time. For comparison, a sample $\nu_\mu \to \nu_e$ oscillation signal expected for the same exposure is also shown corresponding to the best-fit parameters from the Kopp *et al.* analysis [16] of Δm^2=0.43 eV^2, $\sin^2 2\theta_{\mu e}$=0.013. Also shown for comparison is the estimated "electron-like" low energy excess signal [1]. The beam-related background and signal predictions show the overall scale of reconstructed events for 6.6×10^{20} POT (i.e., unlike cosmogenic background numbers, they include an assumed reconstruction efficiency, e.g., 80% and other topological cuts) and include an energy cut of 200 MeV on the reconstructed neutrino energy.

culated and found to be negligible. Out of the total background shown in Table 9, only 10±4 events originate from interactions in the overburden which shows that an overburden of 3 m doesn't increase the overall shower background. Figure 21 (left) shows the end point distribution of all EM particles contained in cosmogenic showers that originate in the overburden. Figure 21 (right) shows the start point distribution of background showers that are daughters of photons created in the overburden.

4.3   Overburden thickness

Although the overburden studies shown in this document are performed using a 3 m thick concrete disc, for technical and cost reasons it is important to determine whether a thinner slab would do a similar job of shielding against cosmogenic backgrounds. To understand the absorption per unit length in the overburden for various particles, one can look at the y projection of the distance between the particle end point and the top of the overburden. Figure 22 shows the distribution of distance of primary and secondary particle end points from the top surface of the overburden for various particle types.
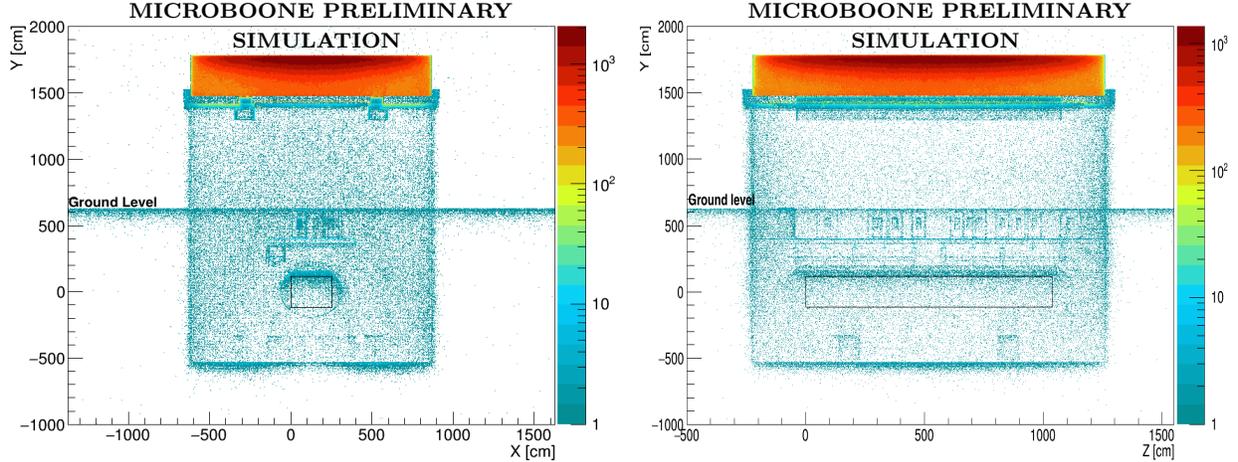
Figure 18: End point distribution of all cosmic particles that are created in the 3 m concrete overburden. Left (right) plot shows the distribution in the YX (YZ) projection of the MicroBooNE TPC. Plots correspond to 10,000 cosmic events (64 seconds of integrated beam spill time).
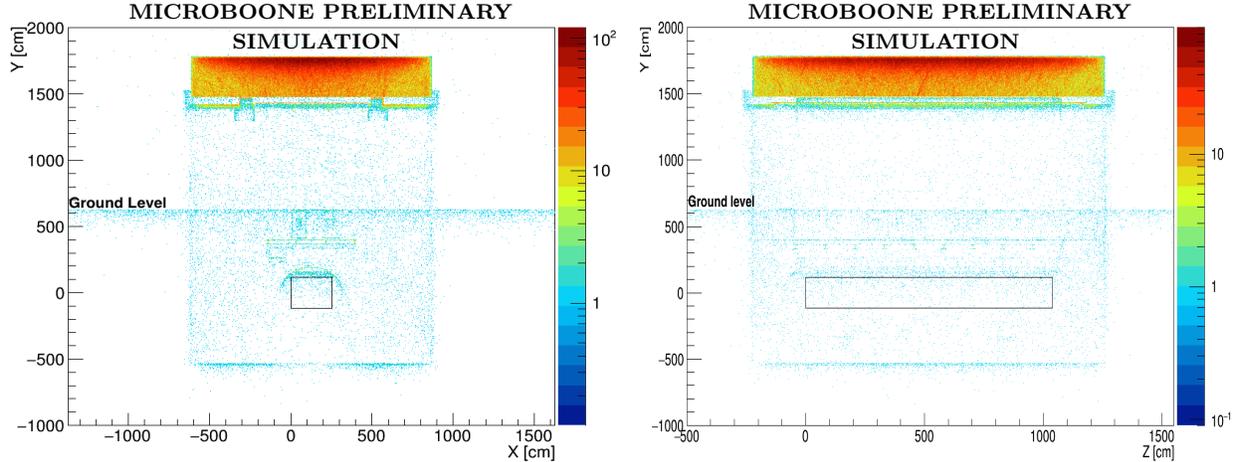

Figure 19: End point distribution of all cosmic particles that are created in the 3 m concrete overburden. A 100 MeV energy cut is applied on all particles. Left (right) plot shows the distribution in the YX (YZ) projection of the MicroBooNE TPC. Plots are made using 10,000 events which correspond to 64 seconds of integrated beam spill time.

From the left column of plots in Figure 22, one can see that in the case of primary particles, an overburden of 1 m (for protons and γ) to 1.5 m (for neutrons) thickness absorbs most of the background. However, the overburden should also be thick enough to reabsorb most of the secondary production from the overburden itself. The right column of plots in Figure 22 show that the effect of an overburden plateaus around 1.5 to 2 m for secondary particles. One can also notice a rise in the secondary backgrounds above 2.5 m. However, as verified in Section 4.2, this doesn't increase the rate of the backgrounds observed in the
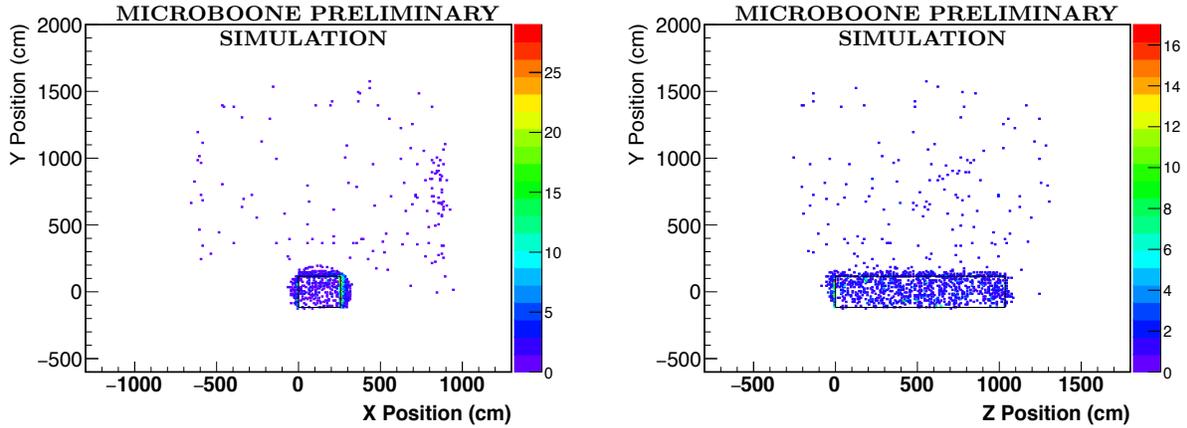
Figure 20: Start point distribution of all secondary photons with energies above 100 MeV that enter the detector in the YX (left) and YZ (right) projection of the MicroBooNE TPC using a data sample with 3 m overburden simulation. A version of these plots without overburden is shown in Figure 12 for comparison.
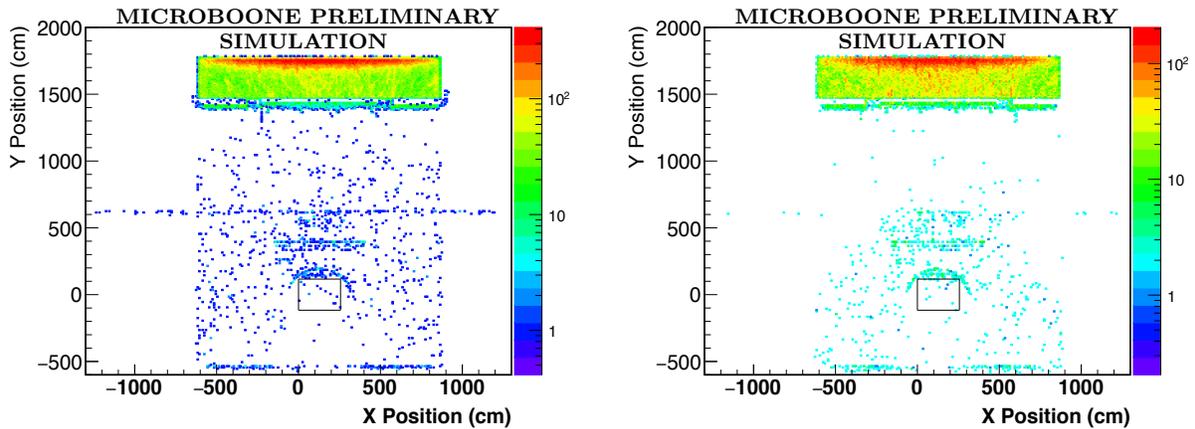

Figure 21: Plots show the distributions in the YX projection of the MicroBooNE TPC. End point distribution of all EM particles contained in background showers that are created in the 3 m concrete overburden (Left). Start point distribution of background showers that are daughters of photons created in the 3 m concrete overburden (Right).

TPC. Please note that the studies shown in this section are preliminary (for example, the particles are not tracked to the TPC and their energies haven't been studied). Detailed studies to understand the necessary thickness of the overburden (1 m, 2 m, or 3 m) and the impact on the shower background are currently being studied. The possibility of using a material other than concrete (such as barite or plastic) or in addition to concrete is also being considered. In addition to this, important technical aspects of overburden installation are also being actively pursued.

(a) Primary neutrons

(b) Secondary neutrons

(c) Primary protons

(d) Secondary protons
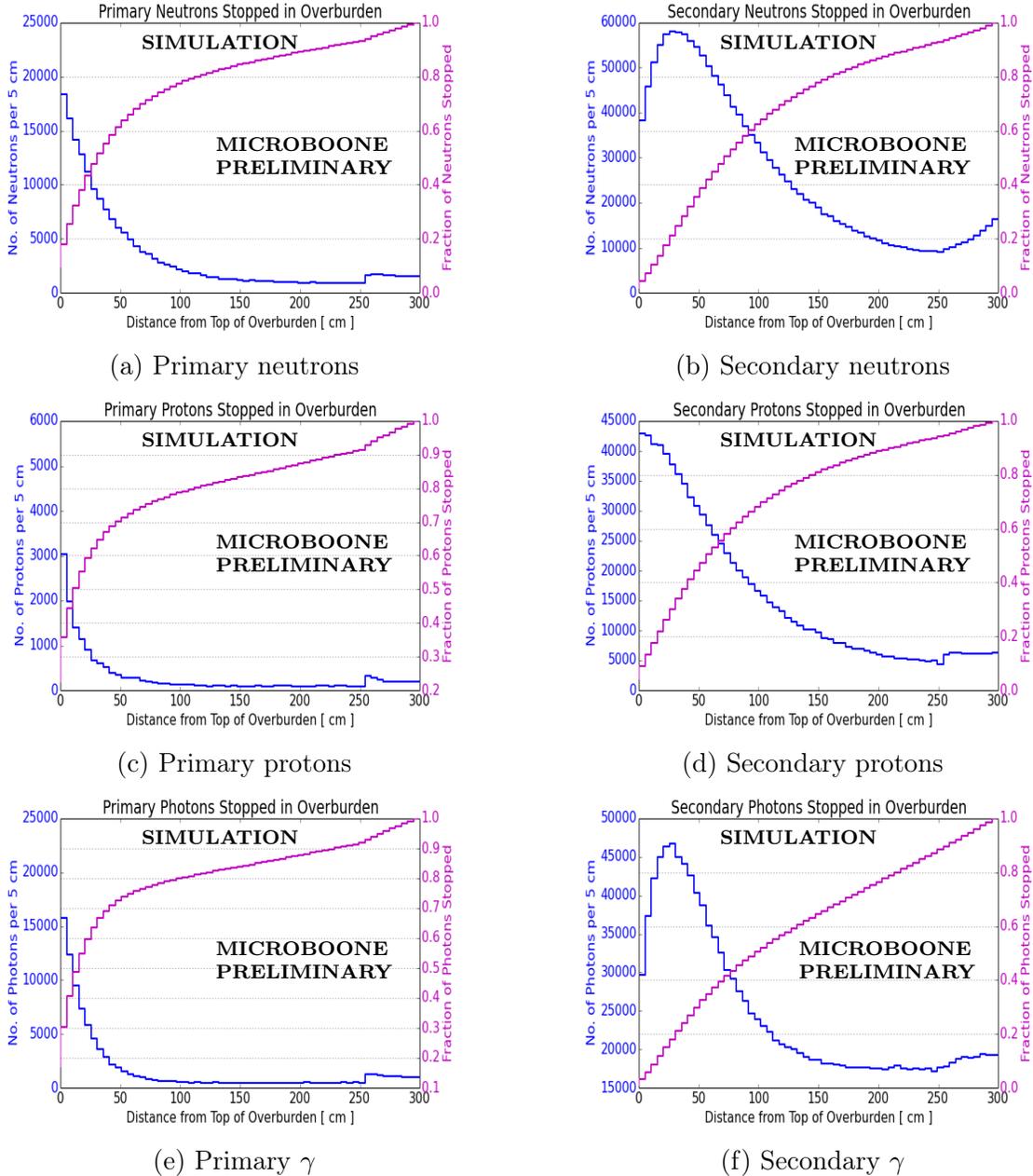
(e) Primary γ

(f) Secondary γ

Figure 22: Distance of end Y positions of various particles from the top surface of the overburden. The set of plots on the left correspond to primary particles and the set of plots on the right correspond to secondary particles. Plots are made using the nominal CORSIKA-CMC-FLUKA sample with 10,000 events. Note that for primary and secondary particles of all types, a 2 m overburden will stop ∼80 to 90% of the particles stopped by a 3 m overburden.

5   Summary and conclusions

Using CORSIKA with the five-component CMC and FLUKA hadron-interaction models, the size of various cosmic backgrounds expected in the MicroBooNE detector is calculated. The

rates are compared to CRY and CORSIKA with other flux and hadron-interaction models as cross-check. We find that the CRY results are similar to those from the CORSIKA-GHEISHA model except that CORSIKA predicts a significant increase in the electromagnetic flux. This increase is primarily due to improved hadronic flux modeling in CORSIKA [15]. In changing from the GHEISHA model to the FLUKA model in CORSIKA the integrated neutron and proton flux (particularly below 1 GeV) increases by a factor of 4.0 and 3.3, respectively. The change from proton-only model to the CMC model increases the muon rate by 40% and neutron rate by a factor of 5.

Using the more accurate CORSIKA-CMC-FLUKA simulation, we find that the predicted cosmogenic shower background induced by non-muon primaries will be worrisome to single-photon searches in MicroBooNE, and contribute non-negligibly as background to the single-electron searches. This prompts consideration of additional shielding through an overburden. Using a 3 m concrete overburden, we find that the overburden significantly (83%) reduces the photon-like "untaggable" shower background making it comparable to the mean number of the signal events. It also marginally (6% for photon-like and 19% for electron-like) reduces the "taggable" shower background (mainly induced by a crossing muon). It is important to note here that only conservative preliminary cuts have been applied in this analysis and thus it is likely that the background be further reduced with additional cuts.

We also studied in detail the effect of a 3 m concrete overburden on various particle rates. The primary motivation of the overburden is to shield non-muon primaries and the backgrounds they generate. The overburden reduces the non-muon primary background by about 76% to 92%. Muons and muon-induced secondaries are mildly reduced by the overburden (by up to about 9%). Most of the particles produced in the overburden are absorbed in it. Only a negligible portion (0.06%) of this background enters the detector.

The ν_e charged-current (CC) oscillation signal ($\sim$70) and low energy excess signal ($\sim$100) shown in this document are calculated assuming 80% flat reconstruction efficiency. The automated reconstruction of showers in data, which is yet to be fully developed, is expected to have less efficiency and resolution than the studies based on MC shown here, in particular for neutrino energies below 200 MeV compounding the effect of cosmogenic shower backgrounds on the ν_e CC oscillation signal. Furthermore, all cosmogenic background shower numbers shown in this document are to be considered as a lower limit as the results assume 100% background rejection out of spill which must be demonstrated on data. Also, cosmic mitigation studies showing good rejection efficiency for cosmogenic background showers are performed with truth-based information and assume a 94% flat efficiency in identifying pair-produced showers. This rejection efficiency will be demonstrated on data.

Given the arguments presented in this section, we find that a concrete overburden of 3 meters would efficiently mitigate cosmic non-muon induced shower backgrounds that are worrisome to low energy excess searches.

References

[1] The MicroBooNE Collaboration, *Technical Design Report*,
`http://www-microboone.fnal.gov/publications/TDRCD3.pdf`, February 2011.

[2] A. A. Aguilar-Arevalo *et al., Unexplained Excess of Electron-like Events from a 1 GeV Neutrino Beam*, Phys. Rev. Lett. **102**, 101802 (2009).

[3] A. A. Aguilar-Arevalo *et al., A Combined* $\nu_\mu \to \nu_e$ *and* $\bar{\nu}_\mu \to \bar{\nu}_e$ *Oscillation Analysis of the MiniBooNE Excesses*, Phys. Rev. Lett. **110**, 161801 (2013).

[4] G. Karageorgi *et al., Description of the MicroBooNE PMT read-out system*, MicroBooNE docdb-2465.

[5] R. Acciarri (3) *et al.,* arXiv:1503.01520 [hep-ex] (2015).

[6] *Cosmic-ray shower generator (CRY) for Monte Carlo transport codes*, Nuclear Science Symposium Conference Record, 2007. NSS '07. IEEE (Volume: 2).
CRY : *http* : *//nuclear.llnl.gov/simulation/main.html*

[7] *CORSIKA an Air Shower Simulation Program*
https : *//web.ikp.kit.edu/corsika/usersguide/usersguide.pdf*

[8] Eric D. Church, *LArSoft: A Software Package for Liquid Argon Time Projection Drift Chambers*,
arXiv:1311.6774 [physics.ins-det].

[9] Robert K Kutschke, *art: A Framework for New, Small Experiments at Fermilab*,
J. Phys.: Conf. Ser. **331** (2011) 032019.

[10] J. F. Ziegler, *Terrestrial cosmic ray intensities*, IMB J. Res. Develop. 42 (1) (January 1998), 117-139.

[11] MCNPX User's Manual, Version 2.5.0, Laurie Waters, *ed.*, LA-CP-05-0369 (2005).
http : *//mcnpx.lanl.gov/documents.html*

[12] National Oceanic and Atmospheric Administration (NOAA)
http://www.ngdc.noaa.gov/geomag-web/

[13] S. Tognini, S. C. Gomes, *CORSIKA Converter Tool*, R. A. HEP Group, Federal University of Goias, Brazil. stognini@fnal.gov and ragomes@if.ufg.br. November 2014.

[14] C. Forti, H. Bilokon, B. d'Ettore Piazzoli, T. K. Gaisser, L. Satta and T. Stanev, *Simulation of atmospheric cascades and deep underground muons*, Phys. Rev. D **42**, 3668 (1990).

[15] Bhadra, Arunava and Ghosh, Sanjay K. and Joarder, Partha S. and Mukherjee, Arindam and Raha, Sibaji, *Study of low energy hadronic interaction models based on BESS observed cosmic ray proton and antiproton spectra at medium high altitude*, Phys. Rev. D **79**, 114027 (2009).

[16] Joachim Kopp, Pedro A. N. Machado, Michele Maltoni, and Thomas Schwetz, *Sterile Neutrino Oscillations: The Global Picture*, JHEP 1305, **050** (2013). arXiv:1303.3011 [hep-ph].

[17] Yun-su Tsai, *Pair production and bremsstrahlung of charged leptons*, Review of Modern Physics, Vol. 46, No. 4, October 1974.

[18] $http://pdg.lbl.gov/2015/AtomicNuclearProperties/HTML/liquid\_argon.html$